International Journal of Solids and Structures 132–133 (2018) 96–104

Contents lists available at ScienceDirect

International Journal of Solids and Structures

journal homepage: www.elsevier.com/locate/ijsolstr

New electromechanical instability modes in dielectric elastomer balloons

Xudong Liang, Shengqiang Cai*

Department of Mechanical and Aerospace Engineering, University of California, San Diego, La Jolla, CA 92093, USA

ARTICLE INFO

Article history:
Received 6 January 2017
Revised 13 September 2017
Available online 18 September 2017

Keywords:
Dielectric elastomer
Balloon
Electromechanical instability
Localized instability

ABSTRACT

Under the actions of internal pressure and electric voltage, a dielectric elastomeric membrane mounted on an air chamber can deform to a balloon shape. Due to the nonlinear deformation, snap-through instability can happen in the balloon, which has been harnessed to achieve giant voltage-triggered deformation. In addition to the snap-through instability, with an applied voltage, a new electromechanical instability mode with a localized bulging-out in the balloon has been recently observed in experiments. However, the reported phenomenon has not been well explained. In this article, through numerical computation, we obtain the relation between the volume of the balloon and its internal pressure, when the balloon is subjected to different voltages. We find out that when the applied voltage is small, the pressure vs. volume diagram of a balloon can be represented by an N-like curve, which is similar to the conventional hyperelastic balloon only subjected internal pressure; when the voltage is larger than a critical value, new instability modes in the balloon emerge, which have a localized bulging-out, similarly to the shape observed in the experiments. We further show that the critical voltage for the new instability mode of the DE balloon is closely associated with the prestretches applied to the membrane and the hyperelastic model for the elastomer.

1. Introduction

Dielectric elastomer (DE) has been regarded as a promising soft active material due to many of their unique properties such as large voltage-induced deformation, low noise during operation, low cost and fast response (Carpi et al., 2011a). In a recent decade, DE has been intensively explored in various applications, including artificial muscle (Kornbluh, 2004; Kwak et al., 2005; Palli and Berselli, 2013; Pelrine et al., 2002), haptic devices (Carpi et al., 2011b; Henann et al., 2013), micro-pumps (Bowers et al., 2011; Goulbourne et al., 2003; Goulbourne et al., 2004; Pope et al., 2004) and adaptive lens (Hwang et al., 2013; Lau et al., 2014; Liang et al., 2014; Son et al., 2012). DE adopted in the aforementioned applications is normally a sandwich structure with a soft elastomeric layer covered by two compliant electrodes on the top and bottom surfaces (Suo, 2010). The elastomer can dramatically reduce its thickness and expand in area when external electric voltage is applied across the thickness direction.

Nonlinear field theory for elastic dielectric accounting for the coupling between mechanics and electricity was originally proposed by Toupin (1956). Relevant studies of elastic dielectric were further developed by Landau (1960), Eringen (1963) and Tiersten (1971). The theory has been re-examined in recent years due to the rapidly growing applications of DE. Constitutive models of DE accounting for large deformation have been developed to explain diverse experimental observations and also provide guidelines for designing new DE devices (Dorfmann and Ogden, 2005; McMeeking and Landis, 2005; Suo et al., 2008).

Among all the DE devices, balloon is one of the most frequently adopted geometries. DE balloons have been successfully developed as spherical-shape actuators and tactile devices (Goulbourne et al., 2003, 2004; Wang et al., 2012). Recently, more applications of DE balloons have been explored due to their unique responses to different electromechanical loadings. Nonlinear vibration with tunable frequency has been demonstrated in spherical DE balloons subjected to a constant pressure and an AC voltage (Zhu et al., 2010). Rudykh and Bhattacharya (2012) predicted snap-through actuation in a thick-walled DE balloon. Liang and Cai (2015) has recently identified inhomogeneous shape bifurcation modes in a spherical DE balloon subjected to internal pressure and a constant electric voltage. Recently, Li et al. (2013) has observed voltage induced snap-through instability in DE balloons. In their experiment, an acrylic elastomer membrane (3MVHB4910), covered by carbon grease over the top and bottom surfaces as soft electrodes, is mounted on an air chamber. The membrane deforms to a balloon shape after air is pumped into the chamber through a valve.

* Corresponding author.
E-mail addresses: shqcai@ucsd.edu, shqcai@gmail.com (S. Cai).

http://dx.doi.org/10.1016/j.ijsolstr.2017.09.021
0020-7683/

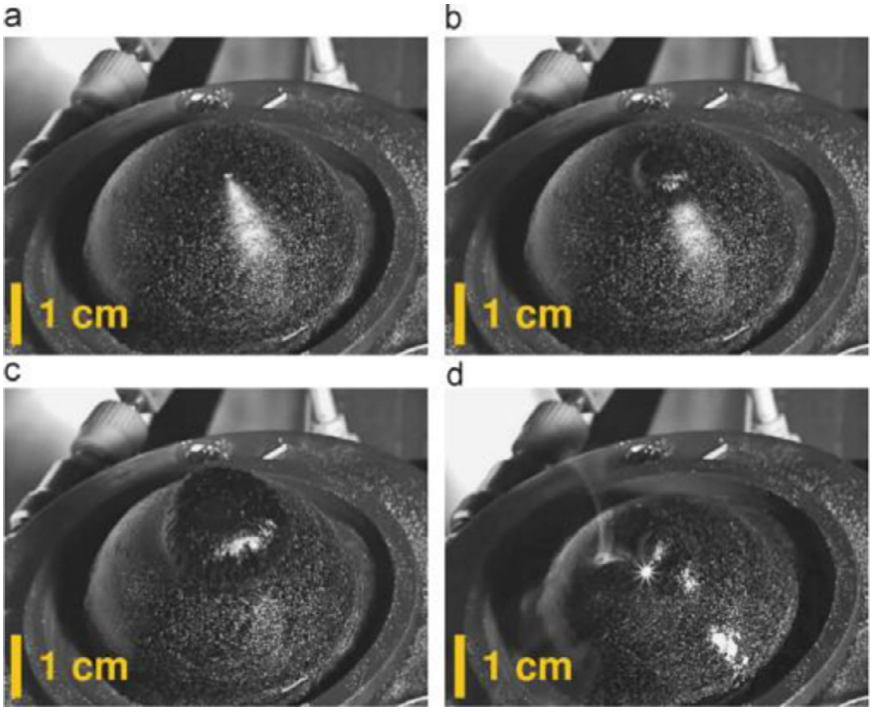

Fig. 1. Experimental observation of localized bulge-out in an inflated DE membrane (Li et al., 2013). In the experiment, a soft DE membrane is mounted on a chamber and air is pumped into the chamber through a valve. The membrane deforms to a balloon shape (a) and the valve is then closed to fix the total amount of air inside the chamber and the balloon. A voltage is subsequently applied to the membrane to further deform the balloon (b-c). When the volume of chamber is small, the apex of the balloon bulges out significantly, which is greatly different from the shape expected from traditional balloon problem. The applied voltage ramps up until the membrane is failed by electrical breakdown (d).

By closing the valve, the amount of air enclosed by the chamber and balloon is fixed, and a voltage is subsequently applied between the electrodes to further deform the DE membrane. Similar to a hyperelastic balloon only subjected to an internal pressure (Alexander, 1971), snap-through instability in a DE balloon was observed due to the non-monotonic relationship between the internal pressure and the volume of the balloon. Additionally, in the experiment, an unusual deformation mode of a DE balloon has been observed (Li et al., 2013). When the volume of the chamber is small, a region on top of the balloon is observed to expand significantly more than its neighboring area (Fig. 1b and c). The area keeps bulging-out as the voltage increases until electrical breakdown happens in the membrane as shown in Fig. 1. Different from the conventional snap-through instability, the new instability mode is more localized around the apex of the balloon, with the rest of membrane almost unperturbed. Such a instability in a balloon has never been reported before in other loading conditions and was also left unexplained in the paper (Li et al., 2013).

In this article, we will study the new instability mode observed in a DE balloon described above. Our numerical calculations show that when the applied voltage is low, the relationship between the internal pressure and volume of a DE balloon is similar to that of a hyperelastic balloon only subjected to an internal pressure, only with quantitative differences; when the applied voltage is high, a new instability mode emerges in the DE balloon for a certain range of pressure. We believe that the new instability mode of the DE balloon is associated with the non-convexity of the free energy density function of DE.

The remainder of the article is organized as follows. Section 2 summarizes the field equations of a DE membrane mounted on a circular hole of an air chamber and subjected to internal pressure and electric voltage. Those equations are solved numerically in Section 3. New instability mode in the balloon with localized bulging-out is identified when the applied voltage is high. In Section 4, we demonstrate that localized bulging-out instability modes of the DE balloon can be affected by pre-stretches and material parameters in the hyperelasticity model. We propose that the new instability mode is associated with the non-convexity of the free energy density function of DE in Section 5. Section 6 summarizes our findings in the article.

2. Inhomogeneous deformation of a DE membrane mounted on an air chamber

To make this article be self-contained, in this section, we summarize the governing equations for a flat DE membrane with homogenous thickness H subjected to internal pressure p and electric voltage Φ as shown in Fig. 2. These equations are mathematically identical to the ones presented in the paper of Li et al. (2013), though the derivation is slightly different. In the problem, an undeformed DE membrane with radius R_0 is mounted over a circular ridge of a chamber, as shown in Fig. 2a. We assume the deformation of the actuated DE balloon is axisymmetric. A Cartesian coordinate system x–z is built upon the apex of the deformed membrane, which coincides with the material point of the center of the undeformed membrane (Fig. 2b). For a point in the undeformed flat membrane: $(X, 0)$, it deforms to (x, z) under electromechanical loading. Consider a material element of the membrane, between two particles X and $X+dX$. When the membrane is in the deformed state, the particle X takes the position of coordinates $x(X)$ and $z(X)$, while the particle $X+dX$ takes the position of coordinates $x(X+dX)$ and $z(X+dX)$. In the undeformed state, the material element is a straight segment, with length dX. In the deformed state, the material element becomes a curved segment, with length $\lambda_1 dX$, where λ_1 is the longitudinal stretch. In a curved state, let $\alpha(X)$ be the slope of a membrane at material particle X. Write

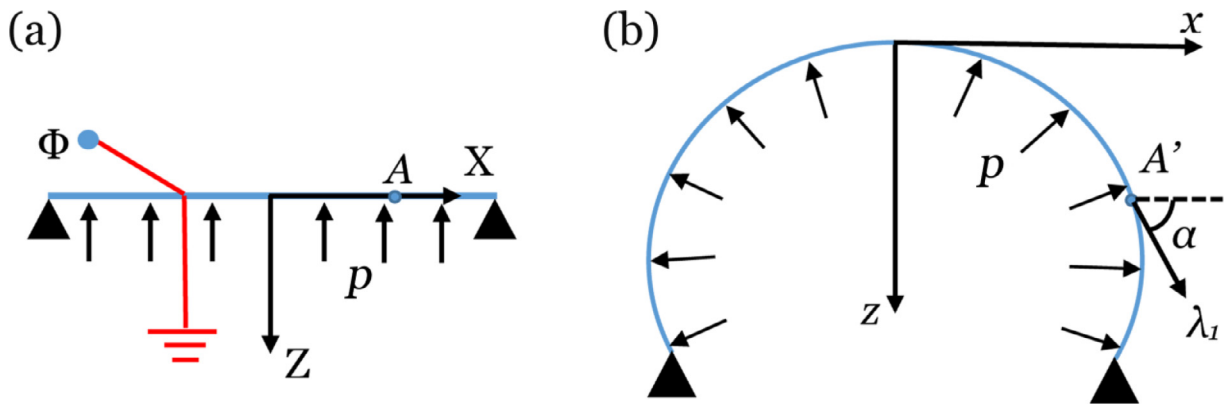

Fig. 2. Schematics of the deformation of dielectric membrane under the action of pressure and applied voltage. (a) Undeformed dielectric membrane. (b) Deformed dielectric membrane.

$dx = x(X+dX) - x(X)$, so that,

$$\frac{dx}{dX} = \lambda_1 \cos\alpha. \tag{1}$$

Similarly, $dz = z(X+dX) - z(X)$, so that,

$$\frac{dz}{dX} = \lambda_1 \sin\alpha. \tag{2}$$

In the undeformed state, a circle of material particles is of a perimeter $2\pi X$. In the deformed state, these material particles occupy a circle of perimeter $2\pi x$. The deformation corresponds to the latitudinal stretch, λ_2. In summary, the two principle stretches in the longitudinal and latitudinal direction in the DE balloon are given by,

$$\lambda_1 = \sqrt{\left(\frac{dx}{dX}\right)^2 + \left(\frac{dz}{dX}\right)^2}, \tag{3}$$

$$\lambda_2 = \frac{x(X)}{X}. \tag{4}$$

Force balance equations of the deformed balloon in the x-direction and the z-directions are given by

$$\frac{d}{dX}(\sigma_1 h x \cos\alpha) + px\frac{dz}{dX} - \frac{\sigma_2 h}{\sin\alpha}\frac{dz}{dX} = 0, \tag{5}$$

$$\frac{d}{dX}(\sigma_1 h x \sin\alpha) - px\frac{dx}{dX} = 0, \tag{6}$$

where σ_1 and σ_2 are the true stresses in the longitudinal direction and latitudinal direction, respectively, p is the internal pressure, and $h(X)$ is the thickness of the deformed DE balloon.

DE is assumed to be incompressible, namely,

$$\lambda_1\lambda_2\lambda_3 = 1, \tag{7}$$

where $\lambda_3 = h(X)/H$ is the stretch in the thickness direction.

Ideal dielectric elastomer model (Zhao et al., 2007) is adopted here by assuming dielectric behavior of an elastomer is exactly the same as that of a polymer melt and the electrical permittivity of DE is not affected by its deformation. We relate the electric displacement D with the electric field E by the following linear equation,

$$D = \varepsilon E, \tag{8}$$

where ε is the electrical permittivity. The electric displacement is equal to the charge density, namely, $D = dQ/da$, where da is the area of the deformed DE membrane and dQ is the correspondent charge accumulated over the area. Electric field in the membrane can be calculated by $E = \Phi/h$, which is inhomogeneous when the thickness of the membrane becomes inhomogeneous.

Using the incompressibility constraint (Eq. (7)), the relations between the true stresses and stretches in the DE membrane can be given by ideal dielectric elastomer model (Suo, 2010; Zhao et al., 2007) as,

$$\sigma_1 - \sigma_3 = \lambda_1\frac{\partial W_s(\lambda_1,\lambda_2)}{\partial\lambda_1} - \varepsilon E^2, \tag{9}$$

$$\sigma_2 - \sigma_3 = \lambda_2\frac{\partial W_s(\lambda_1,\lambda_2)}{\partial\lambda_2} - \varepsilon E^2, \tag{10}$$

where $W_s(\lambda_1, \lambda_2)$ is strain energy density of the elastomer in deformed state with λ_1, λ_2 as its principle stretches, and Gent model (Gent, 1996) is adopted:

$$W_s(\lambda_1,\lambda_2) = -\frac{\mu J_{\lim}}{2}\log\left(1 - \frac{\lambda_1^2 + \lambda_2^2 + \lambda_1^{-2}\lambda_2^{-2} - 3}{J_{\lim}}\right), \tag{11}$$

where μ is the shear modulus for infinitesimal deformation, and $J_{\lim}$ is a constant related to the stretching limit of the elastomer, which is taken to be $J_{\lim} = 270$ and 97.2 in this article (Li et al., 2013; Wang et al., 2016).

Considering the thickness of the DE balloon is much smaller than its radius, the stress in the normal direction of the balloon is negligible compared to the membrane stresses, namely,

$$\sigma_3 = 0. \tag{12}$$

Using the geometric relations in Eqs. (1) and (2) and expressing $d\alpha/dX$, dz/dX and $h = H/\lambda_1\lambda_2$ explicitly, we rewrite the force balance Eqs. (5) and (6) as,

$$\frac{d\alpha}{dX} = -\frac{\sigma_2\lambda_1\sin\alpha}{\sigma_1\lambda_2 X} + \frac{p\lambda_1^2\lambda_2}{\sigma_1 H}, \tag{13}$$

$$\frac{d\lambda_1}{dX} = \left(X\frac{\partial}{\partial\lambda_1}\left(\frac{\sigma_1}{\lambda_1}\right)\right)^{-1} \times\left[\frac{\sigma_2}{\lambda_2}\cos\alpha - \frac{\sigma_1}{\lambda_1} - \frac{\partial}{\partial\lambda_2}\left(\frac{\sigma_1}{\lambda_1}\right)(\lambda_1\cos\alpha - \lambda_2)\right]. \tag{14}$$

The force balance Eqs. (13) and (14), together with the geometric relations (1) and (2), form a set of first-order differential equations that govern the inhomogeneous deformation of the DE membrane. Using the constitutive model in Eqs. (9)–(12) and the definition of the latitudinal stretch in Eq. (2), the right hand side of the governing Eqs. (1), (2), (13) and (14) can be expressed as functions of $x(X)$, $z(X)$, $\lambda_1(X)$ and $\alpha(X)$. The boundary conditions for the DE membrane mounted over an air chamber are prescribed on the apex and the edge of the membrane,

$$x(0) = 0, z(0) = 0, \alpha(0) = 0 \tag{15}$$

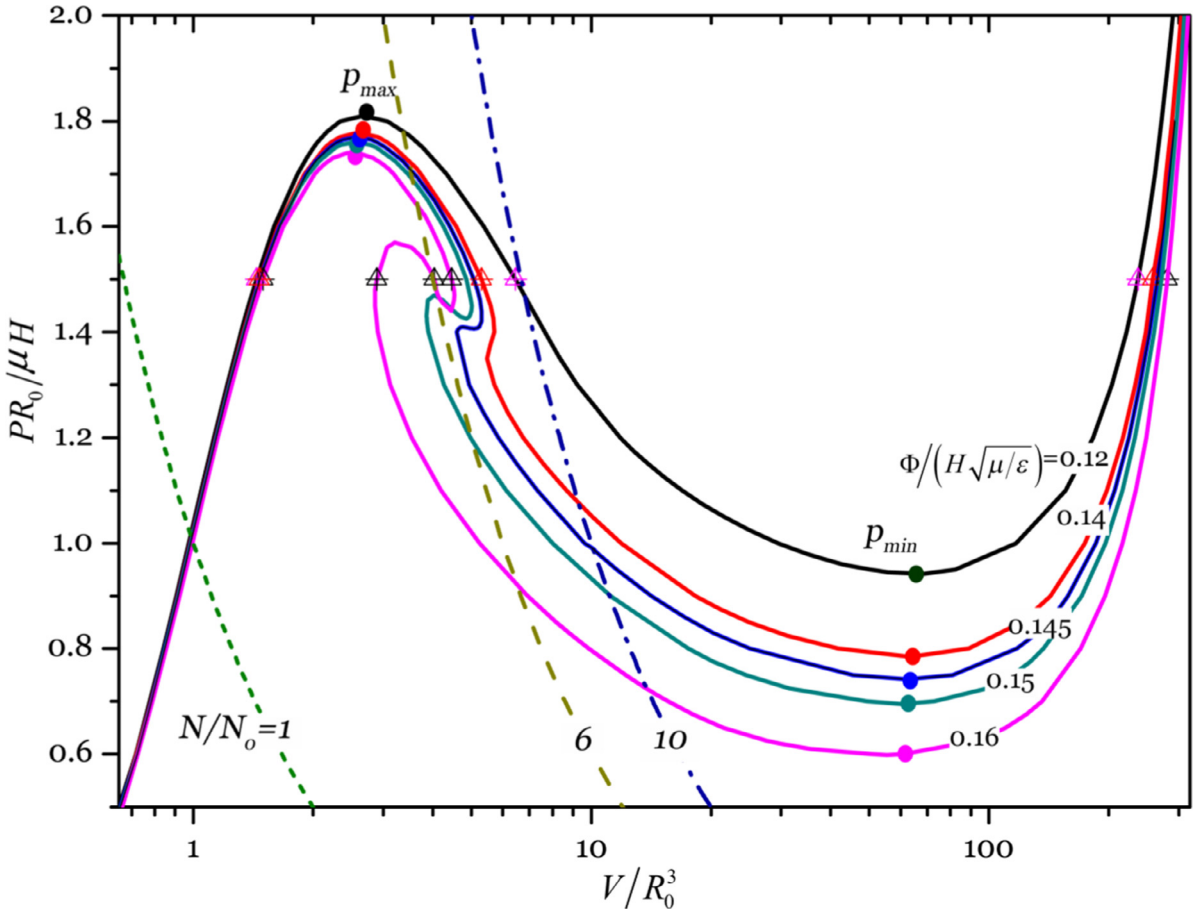

Fig. 3. Pressure vs. volume curve of a DE balloon under several different applied voltages. When the voltage $\Phi/(H\sqrt{\mu/\varepsilon}) < 0.145$, the pressure-volume relationship is represented by an N-like curve. When the voltage $\Phi/(H\sqrt{\mu/\varepsilon}) > 0.145$, a new instability mode of the DE balloon emerges. For a certain range of pressure, five different equilibrium states can be found in the balloon with different volumes. The triangles mark the equilibrium configurations of the DE balloon under the normalized pressure: $pR_0/\mu H = 1.5$. The dash lines describe the state equation of ideal gas under three different amounts of air enclosed in the balloon ($N/N_0 = 1$, 6 and 10), where N_0 is the amount of air molecule when pressure and volume are unity.

$$x(R_0) = R_0. \tag{16}$$

Together with the boundary conditions (15) and (16), the inhomogeneous deformation of the DE membrane subjected to different pressures and voltages can be obtained.

3. Numerical computation of inhomogeneous deformation of the DE membrane

In this section, we conduct numerical calculations to obtain all equilibrium configurations of the DE balloon under the actions of internal pressure and electric voltage, which are governed by the equations formulated in Section 2.

The set of first order differential Eqs. (1), (2), (13) and (14) can be solved numerically by shooting method. Except for the boundary values at the apex: $x(0) = 0$, $z(0) = 0$, and $\alpha(0) = 0$, an value of $\lambda_1(0) = \lambda_a$ is assigned as an additional boundary condition. Those values are used as initial conditions and numerically integrated in Eqs. (1), (2), (13) and (14) to obtain the values of $x(X)$, $z(X)$, $\lambda_1(X)$ and $\alpha(X)$. The value of λ_a is continuously varied until the boundary condition at the edge, $x(R_0) = R_0$, is satisfied.

In Fig. 3, we plot the relation between internal pressure and volume of the DE balloon in equilibrium state with different applied voltages. Pressure, volume and electric voltage are scaled to the dimensionless forms as $pR_0/\mu H$, V/R_0^3 and $\Phi/(H\sqrt{\mu/\varepsilon})$, respectively. The pressure vs. volume diagram of the balloon remains an N-like shape, when the normalized voltage is less than 0.145, similar to the traditional hyperelastic balloon only subjected to pressure (Alexander, 1971; Chen and Healey, 1991; Fu and Xie, 2014; Haughton and Ogden, 1978; Needleman, 1977). If the internal pressure of the balloon is controlled in experiments, when the internal pressure is increased to the first pressure peak in the pressure vs. volume curve: $p_{\max}$, further increase of the pressure will make the DE balloon discontinuously jump from one state with small volume to another state with large volume through snap-through instability. Similarly, when the internal pressure is decreased to the first valley in the pressure vs. volume curve: $p_{\min}$, further decrease of the pressure will make the DE balloon discontinuously jump from a large volume to a small volume. Such snap-through instability has already been widely observed in different experiments. As the normalized voltage exceeds 0.145, additional equilibrium configurations can be obtained in the descending path of pressure vs. volume curve of the balloon as shown in Fig. 3. Consequently, for a certain range of pressure, five different equilibrium states of a DE balloon are found. This is different from the shape bifurcation in a spherical DE balloon, where a non-uniform deformation branch bifurcates from a homogenously deformed state (Fu and Xie, 2014; Liang and Cai, 2015).

We further visualize the deformed shapes and electric field in the DE balloons in Fig. 4. As marked by triangles in the pressure vs. volume curve of the balloon in Fig. 3, the DE balloons are inflated by an internal pressure: $pR_0/\mu H = 1.5$ and the electric voltages $\Phi/(H\sqrt{\mu/\varepsilon})$ ranging from 0.12~0.16. For the voltage smaller

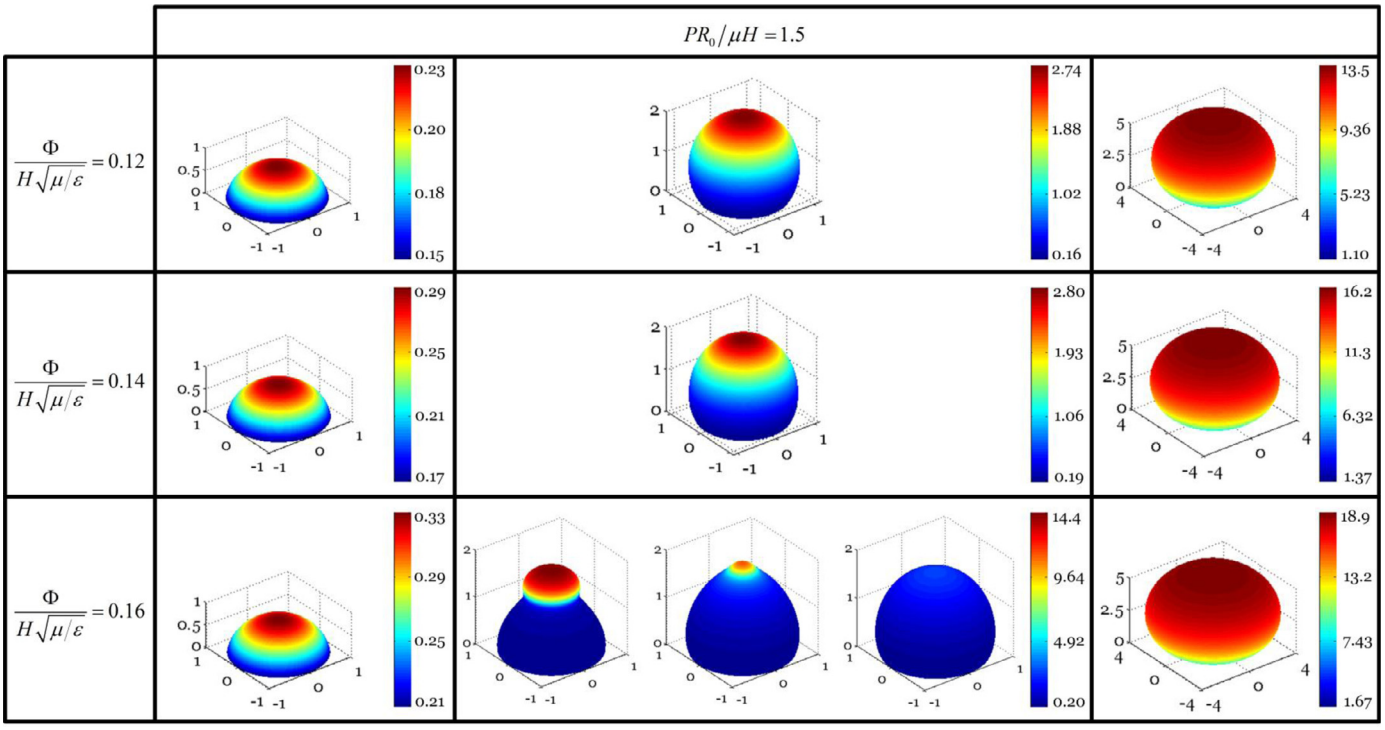

Fig. 4. Deformed shapes and electrical fields in the DE balloons under pressure $pR_0/\mu H = 1.5$. The equilibrium states of the DE balloons are marked with triangles in Fig.3 and arranged by volume (from small to large) in each row. The color stands for the dimensionless true electric field, $E/\sqrt{\mu/\varepsilon}$.

than 0.145, there are three equilibrium configurations under certain pressures. The different shapes of the balloon under the same pressure and voltage have significantly different volumes, which is attributed to the snap-through instability discussed previously. With the increase of the volume, the membrane of the balloon thins down drastically in most part of the balloon, generating a high electric field. By increasing the voltage from 0.12 to 0.14, the deformed shapes of the DE balloons are similar, with only an increase in the volume and the electric filed. However, when the voltage is increased to 0.16, in addition to the deformed shapes observed at lower voltages, two additional configurations emerge. As shown in the third row of Fig. 4, when the applied voltage is 0.16, the first, fourth and fifth configurations of the DE balloon are similar to the lower voltage cases. The second and third configurations of the balloon in the row show different shapes, with localized bulging-out formed around the apex of the balloon, which are similar to what were observed in the experiments (Fig. 1c and b). After forming the localized bulging-out, the volume of the DE balloon decreases compared to the counterpart without the bulging-out, but the electric field at the apex increases dramatically as the membrane thins down greatly. The generation of high electric field accompanied with the formation the bulging-out makes the DE balloon susceptible to electrical breakdown (Li et al., 2013; Liang and Cai, 2015).

Although the balloon with a bulging-out around its apex is an equilibrium state as shown in Fig. 4, it cannot be easily achieved in the experiment with pressure-controlled loading condition (Alexander, 1971; Keplinger et al., 2012; Kyriakides and Yu-Chung, 1990; Li et al., 2013). When the internal pressure reaches the first peak $p_{\max}$ in the pressure vs. volume curve of the balloon, further increase of internal pressure will result in snap-through instability of the balloon as described previously. To reach the equilibrium configurations of the balloon in the descending path of the pressure vs. volume curve, different loading paths need to be adopted in the experiment. As described in the paper (Li et al., 2013), the new instability mode of the balloon can be observed when the applied voltage is increased while the total amount of air enclosed by the balloon is fixed. To obtain the relation between the applied and the volume of the balloon, we simply need to introduce the ideal gas law as the state equation of the enclosed air:

$$Nk_BT = (p + p_{atm})(V + V_c), \tag{17}$$

where p is the excessive internal pressure of the enclosed air in the balloon relative to the atmospheric pressure p_{atm}, V and V_c are the volume of the balloon and the air chamber, respectively, N is the number of the gas molecule, k_B is the Boltzmann constant and T is the temperature. The amount of the air molecules in the chamber and balloon is fixed after the valve is closed in the experiment, and it is scaled as N/N_0, where N_0 is the number of molecules when dimensionless pressure and volume are unity.

Without losing generality, we assume the deformation of the balloon is isothermal, the volume of the chamber $V_c = 0$ in the following analysis. By selecting different amount of air enclosed in the balloon, the curves describing the state equation of ideal gas (Eq. (17)) are sketched as dash lines in Fig. 3. The crossing points between the curves describing the state equation of ideal gas and the pressure vs. volume curves of the DE balloon represent the equilibrium configurations of the DE balloon with certain amount of enclosed air. By selecting the crossing points, we can obtain the relations between the applied-voltage vs. volume of the DE balloons with fixed amount of enclosed air as plotted in Fig. 5. For a small amount of enclosed air ($N/N_0 = 1$), the excessive internal pressure p is smaller than the first pressure peak p_{max} in the pressure vs. volume curve. The balloon is slightly inflated and relatively stiff toward expansion. Consequently, increase of the applied voltage results in a small change of balloon volume. For a large amount of air ($N/N_0 = 10$), the curve describing the state equation of ideal gas also only intersects with the pressure vs. volume curve of the DE balloon at one point for one applied voltage. However, the stiffness of DE balloon decreases a lot with a large volume. A small

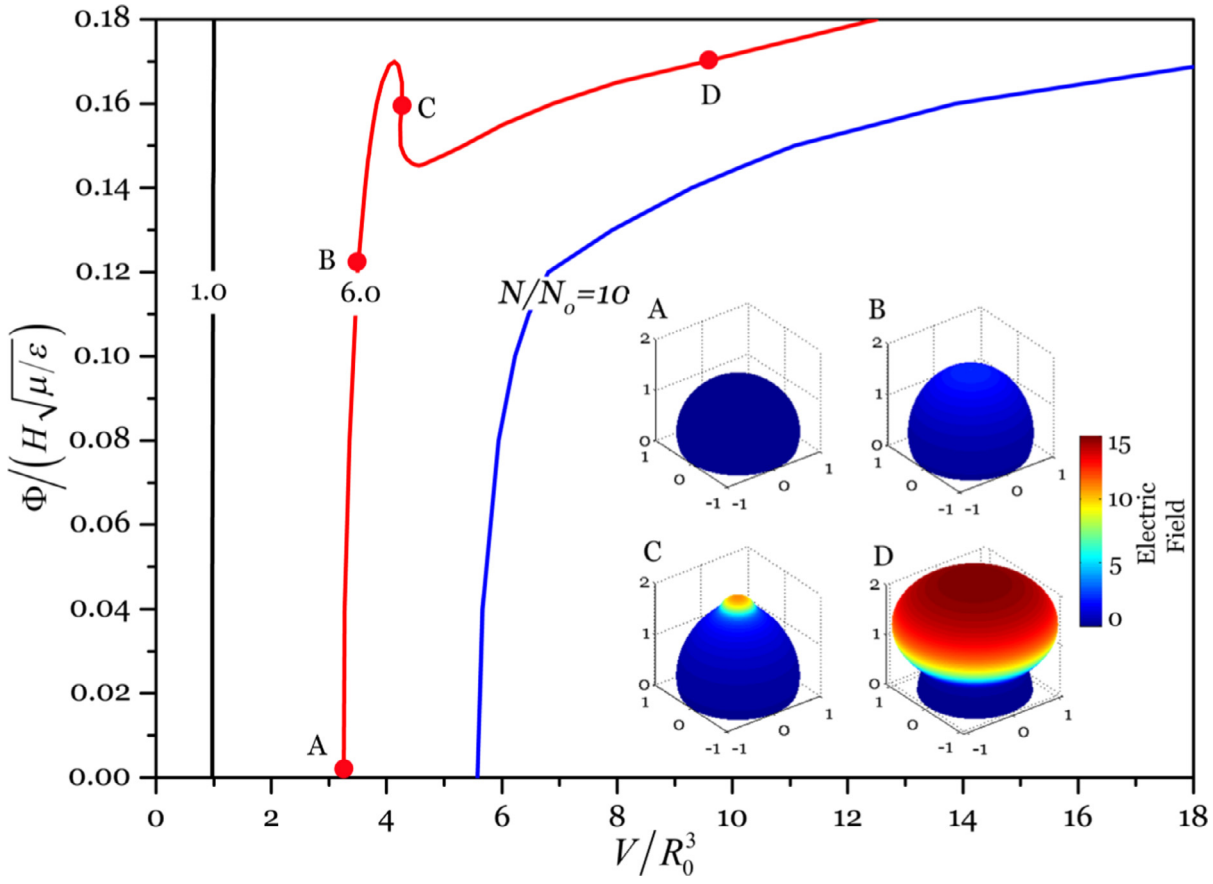

Fig. 5. Voltage vs. volume curve for the DE balloon with different amounts of enclosed air. The number of air molecule N is normalized by N_0, which is the number of molecule when the normalized pressure and volume are unity. The voltage-volume relation is monotonic for small ($N/N_0 = 1$) and large ($N/N_0 = 10$) amount of air, while non-monotonic for $N/N_0 = 6$. The deformed shapes and electric field with varied loading conditions (A~D) in the DE balloon are plotted in the inset.

increase of voltage can result in large volume change of the balloon as shown in Fig. 5, which was also demonstrated in the experiments (Keplinger et al., 2012; Li et al., 2013). For an intermediate amount of enclosed air with $N/N_0 = 6$, the curve describing the state equation of ideal gas may intersect with pressure vs. volume curves of the balloon at multiple points for a given voltage. In another word, for a fixed amount of enclosed air and applied voltage, multiple equilibrium states of the balloon may exist. We plot several deformed shapes and electric field in the DE balloons with varied loading conditions (A~D) in the inset of Fig. 5. To determine if any configurations of the DE balloon is stable or not, perturbation analyses are necessary, which is beyond the scope of the current article.

Last, we compared the electric breakdown field of the material to the true electric fields in the DE balloon of different shapes. It is apparent that if the bulging-out shape of the DE balloon is physically realizable, the maximum electric field in the balloon has to be lower than the electric breakdown field of the DE material. Given that the DE material used in the experiment (Li et al., 2013) was VHB 4910, we use the following representative values of shear modulus $\mu = 10 \sim 45\,kPa$, the dielectric constant $\varepsilon = 4.16 \times 10^{-11}\,F/m$ and the electric breakdown field $E_B = 2.18 \times 10^8\,V/m$ (Plante and Dubowsky, 2006; Wang et al., 2016; Zhao and Suo, 2010). The dimensionless electric breakdown field can be estimated as $E_B/\sqrt{\mu/\varepsilon} = 6.7 \sim 10$. The maximum electric field in some DE balloons with bulging-out configurations shown in Fig. 4 and inset of Fig. 5 are slightly smaller than or comparable to the electric breakdown field. This is consistent with the experimental observations that the formation of localized bulging-out often quickly results in the failure of the material (Li et al., 2013).

4. Effects of prestretches and stretching limit on the new instability modes

Actuating behavior of DE can be greatly affected by its prestretches (Ha et al., 2006; Huang et al., 2012; Kofod, 2008; Pelrine et al., 2000; Wissler and Mazza, 2005). In particular, electromechanical instability in a DE membrane can be delayed or even eliminated by applying prestretches. Consequently, for most applications of DE devices, prestretches are often applied onto the material. In this section, we first study the effects of prestretches in the DE membrane on the new bulging-out instability modes of the DE balloon.

As shown in the inset of Fig. 6, the DE membrane is of flat circular shape with radius R_0 in the reference state, and is prestretched equal-biaxially and held by a rigid ring before actuation. The pressure vs. volume curves of equilibrium states of a DE balloon are shown in Fig. 6 with prestretch $\lambda_p = 2$. By comparing Fig. 6 with Fig. 3, we can clearly see the effects of prestretches on the actuation behavior of a DE balloon. With the applied prestretch, when the dimensionless voltage $\Phi/(H\sqrt{\mu/\varepsilon}) < 0.14$, the internal pressure applied to the balloon increases monotonically with its volume; no snap-through instability is expected, which is in direct contrast to the results shown in Fig. 3. When $0.14 < \Phi/(H\sqrt{\mu/\varepsilon}) < 0.17$, the pressure vs. volume relationship becomes non-monotonic. For such a range of voltage, a DE balloon can undergo snap-through instability as it jumps from one state

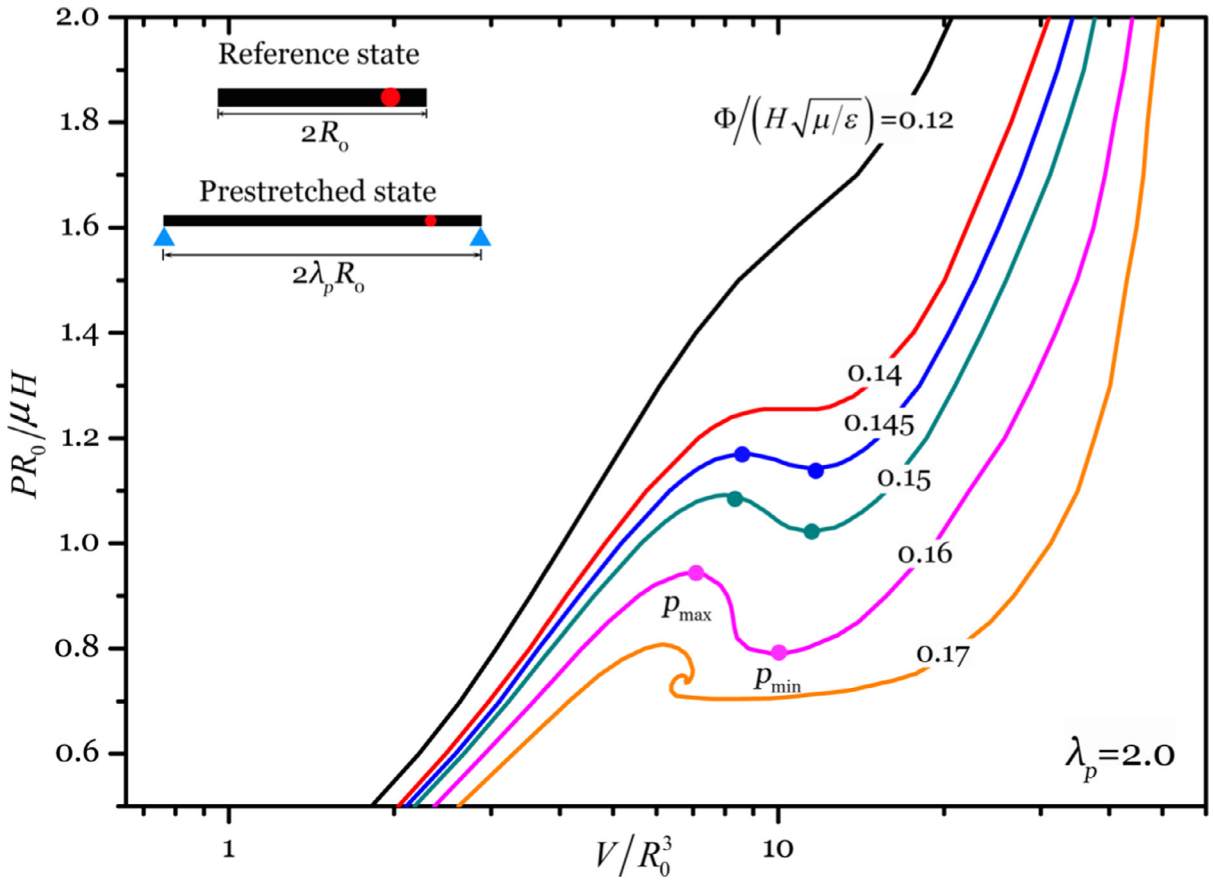

Fig. 6. Pressure vs. volume curves of a DE balloon with prestretch $\lambda_p = 2.0$ as shown in the inset. Both snap-through and localized bulging out instability modes are delayed by prestretches on the DE membrane. For dimensionless voltage $\Phi/(H\sqrt{\mu/\varepsilon}) < 0.14$, the pressure increases monotonically with the volume. For $0.14 < \Phi/(H\sqrt{\mu/\varepsilon}) < 0.17$, the pressure vs. volume curves remain N-shape, with three equilibrium configurations within a range of pressures. For $\Phi/(H\sqrt{\mu/\varepsilon}) = 0.17$, two additional configurations emerge as the localized bulging-out configurations for certain pressures.

to another at the local maximum or minimum pressures (p_{max} and p_{min}). However, the volume change of a DE balloon is much smaller than the one without prestretch as shown in Fig. 3. The additional configurations, which correspond to the localized bulging-out, only appear when $\Phi/(H\sqrt{\mu/\varepsilon})$ is further increased to 0.17. The emergence of the new instability mode with bulging-out shape requires a higher voltage when prestretches are applied. Consequently, the DE material is prone to electric breakdown due to the application of prestretch. Therefore, our results show that prestretches can be used to tune the critical voltages for both snap-through instability and the emergence of the bulging-out instability modes of a DE balloon subject to electromechanical loading.

Different hyperelastic models have been used in DE model to interpret different experimental results (Li et al., 2013; Liang and Cai, 2015; Wang et al., 2016; Xie et al., 2016). Even with the same hyperelastic model, different material parameters have been adopted. For example, recent experimental measurements of acrylic elastomer (VHB 4910) which is used in the referred experiments (Li et al., 2013), revealed a stretching limit $\lambda_{lim} \sim 9.0$ under quasi-static (low stretch-rate), monotonic simple tension test (Wang et al., 2016), corresponding to the value of $J_{lim} = 97.2$ in Gent model. The value of J_{lim} is much smaller than the one used in the previous studies (Li et al., 2013) and the aforementioned numerical computation ($J_{lim} = 270$). Therefore, in the section, we next study the effects of material parameter J_{lim} on the actuating behavior of DE balloon.

An elastomer with smaller value of J_{lim} shows stiffening effect at smaller stretches. To reveal the effects of J_{lim} on the actuating behavior of a DE balloon, we carried out simulations with $J_{lim} = 97.2$ and compared the results to the one with $J_{lim} = 270$. As shown in Fig. 7, the pressure vs. volume curves of a DE balloon share a similar shape under pressure and electric field as shown in Fig. 3. When the voltage is lower than a critical value (~0.25), the pressure-volume curve remains an N-shape curve; when voltage is higher than the critical value, two additional configurations emerge with the localized bulging-out for certain pressure. Similar to the effect of prestretch, reducing the value of J_{lim} also increases the voltage for triggering the bulging-out instability mode.

5. Non-convex free energy and new instability modes in DE balloon

For an elastomeric balloon, the relationship between its internal pressure and volume can be usually represented by an N-like curve (Fu and Xie, 2010; Haughton and Ogden, 1978; Needleman, 1977), which often results in snap-through instability of the balloon in experiments (Alexander, 1971; Kyriakides and Yu-Chung, 1990). Such a non-monotonic relationship between the internal pressure and volume of a balloon is due to its large and nonlinear deformation instead of any special constitutive model of the elastomer. Explicitly speaking, strain energy density functions of an elastomer given by different constitutive models are typically convex (Haughton and Ogden, 1978; Suo, 2010). As a result, similar N-like curves between the pressure and volume have also been theoretically predicted (Li et al., 2013; Liang et al., 2014) and experimentally validated (Keplinger et al., 2012; Li et al., 2013) for a DE balloon subjected to a constant voltage across its thickness.

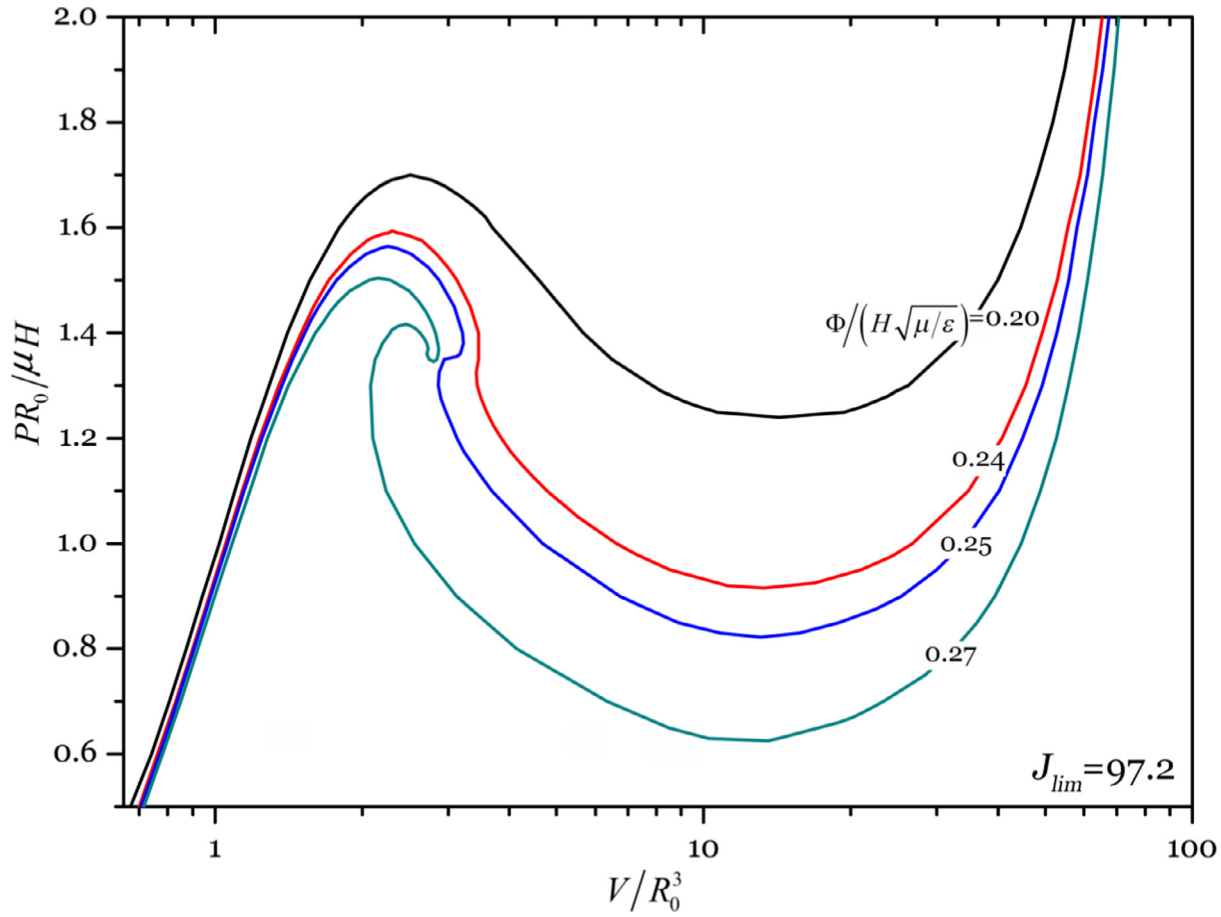

Fig. 7. Pressure vs. volume curves of a DE balloon with smaller stretch limit as $J_{\text{lim}} = 97.2$. When the voltage $\Phi/(H\sqrt{\mu/\varepsilon}) < 0.25$, the pressure-volume relationship is represented by an N-like curve. When $\Phi/(H\sqrt{\mu/\varepsilon}) > 0.25$, new instability modes with bulging-out of the DE balloon emerge. The voltage required for the emergence of the bulging-out instability mode increases when J_{lim} of the elastomer is reduced from 270 to 97.2.

However, it is known that free energy density function of a DE membrane may become non-convex when the applied voltage is high, which can lead to electromechanical instability of a DE membrane with homogenous deformation (Zhao et al., 2007; Zhao and Suo, 2007). We believe the additional instability modes of the DE balloon observed in the experiment and captured by our numerical computation in Section 3 are due to the non-convexity of the free energy density function of the DE membrane when the applied voltage is high.

The convexity of free energy density function of a DE membrane can be assessed by computing its Hessian (Appendix A1). As shown in Fig. A1, each curve represents a critical condition when the free energy density function of becomes non-convex. The global minimum of the contour plots stays at the voltage: $\Phi_{\min} = 0.123H\sqrt{\mu/\varepsilon}$ for DE with $J_{\text{lim}} = 270$, and $\Phi_{\min} = 0.2085H\sqrt{\mu/\varepsilon}$ for DE with $J_{\text{lim}} = 97.2$. When the applied voltage$\Phi < \Phi_{\min}$, the free energy density function of the DE is convex for any deformation state; when the applied voltage is larger than $\Phi_{\min}$, the free energy density function of the DE becomes non-convex for certain deformation state, which is believed to be the main reason for the emergence of the bulging-out configuration of the DE balloon.

It is noted that in this article, we do not intend to precisely predict the onset of the newly observed bulging-out instability by evaluating Hessian, which is only valid for predicting critical conditions for instability with homogeneous deformation (Dorfmann and Ogden, 2014; Suo, 2010). To predict onset of instability of a structure with inhomogeneous deformation or other fields, perturbation analyses may be required (Dorfmann and Ogden, 2010; Dorfmann and Ogden, 2014; Fu and Xie, 2014; Liang and Cai, 2015). In the paper, we would like to propose that the additional bulging-out instability modes of the DE balloon are associated with its non-convex free energy density function of DE at high voltage.

6. Concluding remarks

In this article, we have studied new instability modes in a DE balloon subjected to internal pressure and electric voltage. By numerically solving the governing equations, we obtain the equilibrium configurations of a DE balloon under different internal pressures and voltages. We find out that when the applied voltage is small, the pressure vs. volume diagram of a DE balloon can be represented by an N-like curve, which is similar to the conventional hyperelastic balloon problem; when the voltage is larger than a critical value, new instability modes in the balloon emerge, which have an abnormal localized bulging-out, similar to the shape observed previously (Li et al., 2013). Based on our numerical calculations, we show that the bulging-out modes recently observed in a DE balloon can be an equilibrium configuration. Such a bulging-out shape does not rely on any specific material or geometrical defects. In addition, the prediction of the bulging-out configuration does not require any modifications of the DE balloon model. We further show that the DE balloon with a bulging-out shape can be realized in the experiment by gradually increasing the applied voltage while fixing the total amount of air enclosed in the balloon. We believe the bulging-out instability modes of a DE balloon are related to the non-convexity of the free energy density func-

tion of DE when the applied voltage is high. We finally show that prestretch as well as the material parameter ($J_{\lim}$) can affect the voltage required for triggering the emergence of the bulging-out instability of a DE balloon.

Acknowledgments

The work is supported by the National Science Foundation through Grant No. CMMI-1554212.

During the reviewing period of this manuscript, a paper on the same subject appeared in the Journal of Mechanics and Physics of Solids (Wang et al., 2017). The two works were performed independently, but both were inspired by the experimental observations reported in Li et al. (2013). The two papers were submitted approximately at the same time in January 2017.

Supplementary materials

Supplementary material associated with this article can be found, in the online version, at doi:10.1016/j.ijsolstr.2017.09.021.

References

Alexander, H., 1971. Tensile instability of initially spherical balloons. Int. J. Eng. Sci. 9, 151–160.
Bowers, A.E., Rossiter, J.M., Walters, P.J., Ieropoulos, I.A., 2011. Dielectric elastomer pump for artificial organisms, SPIE smart structures and materials+ nondestructive evaluation and health monitoring. Int. Soc. Opt. Photon. 797629-797629-797627.
Carpi, F., De Rossi, D., Kornbluh, R., Pelrine, R.E., Sommer-Larsen, P., 2011a. Dielectric Elastomers as Electromechanical Transducers: Fundamentals, Materials, Devices, Models and Applications of an Emerging Electroactive Polymer Technology. Elsevier.
Carpi, F., Frediani, G., De Rossi, D., 2011b. Opportunities of hydrostatically coupled dielectric elastomer actuators for haptic interfaces, SPIE smart structures and materials+ nondestructive evaluation and health monitoring. Int. Soc. Opt. Photon. 797618-797618-797619.
Chen, Y.-C., Healey, T.J., 1991. Bifurcation to pear-shaped equilibria of pressurized spherical membranes. Int. J. Non-Linear Mech. 26, 279–291.
Dorfmann, A., Ogden, R., 2005. Nonlinear electroelasticity. Acta Mech. 174, 167–183.
Dorfmann, A., Ogden, R., 2010. Nonlinear electroelastostatics: incremental equations and stability. Int. J. Eng. Sci. 48, 1–14.
Dorfmann, L., Ogden, R.W., 2014. Instabilities of an electroelastic plate. Int. J. Eng. Sci. 77, 79–101.
Eringen, A.C., 1963. On the foundations of electroelastostatics. Int. J. Eng. Sci. 1, 127–153.
Fu, Y., Xie, Y., 2010. Stability of localized bulging in inflated membrane tubes under volume control. Int. J. Eng. Sci. 48, 1242–1252.
Fu, Y., Xie, Y., 2014. Stability of pear-shaped configurations bifurcated from a pressurized spherical balloon. J. Mech. Phys. Solids 68, 33–44.
Gent, A., 1996. A new constitutive relation for rubber. Rubber Chem. Technol. 69, 59–61.
Goulbourne, N., Frecker, M.I., Mockensturm, E.M., Snyder, A.J., 2003. Modeling of a dielectric elastomer diaphragm for a prosthetic blood pump, smart structures and materials. Int. Soc. Opt. Photon. 319–331.
Goulbourne, N.C., Frecker, M.I., Mockensturm, E., 2004. Electro-elastic modeling of a dielectric elastomer diaphragm for a prosthetic blood pump, smart structures and materials. Int. Soc. Opt. Photon. 122–133.
Ha, S.M., Yuan, W., Pei, Q., Pelrine, R., Stanford, S., 2006. Interpenetrating polymer networks for high-performance electroelastomer artificial muscles. Adv. Mater. 18, 887–891.
Haughton, D., Ogden, R., 1978. On the incremental equations in non-linear elasticity—I. Membrane theory. J. Mech. Phys. Solids 26, 93–110.
Henann, D.L., Chester, S.A., Bertoldi, K., 2013. Modeling of dielectric elastomers: Design of actuators and energy harvesting devices. J. Mech. Phys. Solids 61, 2047–2066.
Huang, J., Li, T., Chiang Foo, C., Zhu, J., Clarke, D.R., Suo, Z., 2012. Giant, voltage-actuated deformation of a dielectric elastomer under dead load. Appl. Phys. Lett. 100, 041911.
Hwang, T., Kwon, H.-Y., Oh, J.-S., Hong, J.-P., Hong, S.-C., Lee, Y., Choi, H.R., Kim, K.J., Bhuiya, M.H., Nam, J.-D., 2013. Transparent actuator made with few layer graphene electrode and dielectric elastomer, for variable focus lens. Appl. Phys. Lett. 103, 023106.
Keplinger, C., Li, T., Baumgartner, R., Suo, Z., Bauer, S., 2012. Harnessing snap-through instability in soft dielectrics to achieve giant voltage-triggered deformation. Soft Matter 8, 285–288.
Kofod, G., 2008. The static actuation of dielectric elastomer actuators: how does pre-stretch improve actuation? J. Phys. D 41, 215405.
Kornbluh, R., 2004. Dielectric elastomer artificial muscle for actuation, sensing, generation, and intelligent structures. Mater. Technol. 19, 216–223.
Kwak, J.W., Chi, H.J., Jung, K.M., Koo, J.C., Jeon, J.W., Lee, Y., Ryew, Y., Choi, H.R., 2005. A face robot actuated with artificial muscle based on dielectric elastomer. J. MechSci. Technol. 19, 578–588.
Kyriakides, S., Yu-Chung, C., 1990. On the inflation of a long elastic tube in the presence of axial load. Int. J. Solids Struct. 26, 975–991.
Landau, L.D., 1960. EM Lifshitz Electrodynamics of continuous media. Course Theor. Phys. 8, 15.
Lau, G.-K., La, T.-G., Shiau, L.-L., Tan, A.W.Y., 2014. Challenges of using dielectric elastomer actuators to tune liquid lens. In: Proc. SPIE, p. 90561J.
Li, T., Keplinger, C., Baumgartner, R., Bauer, S., Yang, W., Suo, Z., 2013. Giant voltage-induced deformation in dielectric elastomers near the verge of snap-through instability. J. Mech. Phys. Solids 61, 611–628.
Liang, D., Lin, Z.-F., Huang, C.-C., Shih, W.-P., 2014. Tunable lens driven by dielectric elastomer actuator with ionic electrodes. IET Micro Nano Lett. 9, 869–873.
Liang, X., Cai, S., 2015. Shape bifurcation of a spherical dielectric elastomer balloon under the actions of internal pressure and electric voltage. J. Appl. Mech. 82, 101002.
McMeeking, R.M., Landis, C.M., 2005. Electrostatic forces and stored energy for deformable dielectric materials. J. Appl. Mech. 72, 581–590.
Needleman, A., 1977. Inflation of spherical rubber balloons. Int. J. Solids Struct. 13, 409–421.
Palli, G., Berselli, G., 2013. On the control of a dielectric elastomer artificial muscle with variable impedance, ASME 2013 conference on smart materials, adaptive structures and intelligent systems. Am. Soc. Mech. Eng. V001T003A042-V001T003A042.
Pelrine, R., Kornbluh, R., Pei, Q., Joseph, J., 2000. High-speed electrically actuated elastomers with strain greater than 100%. Science 287, 836–839.
Pelrine, R., Kornbluh, R.D., Pei, Q., Stanford, S., Oh, S., Eckerle, J., Full, R.J., Rosenthal, M.A., Meijer, K., 2002. Dielectric elastomer artificial muscle actuators: toward biomimetic motion, SPIE's 9th annual international symposium on smart structures and materials. Int. Soc. Opt. Photon. 126–137.
Plante, J.-S., Dubowsky, S., 2006. Large-scale failure modes of dielectric elastomer actuators. Int. J. Solids Struct. 43, 7727–7751.
Pope, K., Tews, A., Frecker, M.I., Mockensturm, E., Goulbourne, N.C., Snyder, A.J., 2004. Dielectric elastomer laminates for active membrane pump applications, smart structures and materials. Int. Soc. Opt. Photon. 60–67.
Rudykh, S., Bhattacharya, K., 2012. Snap-through actuation of thick-wall electroactive balloons. Int. J. Non-Linear Mech. 47, 206–209.
Son, S.-i., Pugal, D., Hwang, T., Choi, H.R., Koo, J.C., Lee, Y., Kim, K., Nam, J.-D., 2012. Electromechanically driven variable-focus lens based on transparent dielectric elastomer. Appl. Opt. 51, 2987–2996.
Suo, Z., 2010. Theory of dielectric elastomers. Acta Mech. Solida Sinica 23, 549–578.
Suo, Z., Zhao, X., Greene, W.H., 2008. A nonlinear field theory of deformable dielectrics. J. Mech. Phys. Solids 56, 467–486.
Tiersten, H., 1971. On the nonlinear equations of thermo-electroelasticity. Int. J. Eng. Sci. 9, 587–604.
Toupin, R.A., 1956. The elastic dielectric. J. Ration. Mech. Anal. 5, 849–915.
Wang, F., Yuan, C., Lu, T., Wang, T., 2017. Anomalous bulging behaviors of a dielectric elastomer balloon under internal pressure and electric actuation. J. Mech. Phys. Solids 102, 1–16.
Wang, H., Cai, S., Carpi, F., Suo, Z., 2012. Computational model of hydrostatically coupled dielectric elastomer actuators. J. Appl. Mech. 79, 031008.
Wang, S., Decker, M., Henann, D.L., Chester, S.A., 2016. Modeling of dielectric viscoelastomers with application to electromechanical instabilities. J. Mech. Phys. Solids 95, 213–229.
Wissler, M., Mazza, E., 2005. Modeling of a pre-strained circular actuator made of dielectric elastomers. Sensors Actuators A 120, 184–192.
Xie, Y.-X., Liu, J.-C., Fu, Y., 2016. Bifurcation of a dielectric elastomer balloon under pressurized inflation and electric actuation. Int. J.Solids Struct. 78, 182–188.
Zhao, X., Hong, W., Suo, Z., 2007. Electromechanical hysteresis and coexistent states in dielectric elastomers. Phys. Rev. B 76, 134113.
Zhao, X., Suo, Z., 2007. Method to analyze electromechanical stability of dielectric elastomers. Appl. Phys. Lett. 91, 061921.
Zhao, X., Suo, Z., 2010. Theory of dielectric elastomers capable of giant deformation of actuation. Phys. Rev. Lett. 104, 178302.
Zhu, J., Cai, S., Suo, Z., 2010. Nonlinear oscillation of a dielectric elastomer balloon. Polymer Int. 59, 378–383.